

LatentFM: A Latent Flow Matching Approach for Generative Medical Image Segmentation

Trinh Ngoc Huynh, Nguyen Kim Hoang Anh, Nguyen Hai Toan, Tran Quoc Long

Institute for Artificial Intelligence

University of Engineering & Technology (VNU-UET)

Hanoi, VietNam

huynhntn@vnu.edu.vn, hoanganhnh1604@gmail.com, nguyenhaitoan@vnu.edu.vn, tqlong@vnu.edu.vn

Abstract—Generative models have achieved remarkable progress with the emergence of flow matching (FM). It has demonstrated strong generative capabilities and attracted significant attention as a simulation-free flow-based framework capable of learning exact data densities. Motivated by these advances, we propose LatentFM, a flow-based model operating in the latent space for medical image segmentation. To model the data distribution, we first design two variational autoencoders (VAEs) to encode both medical images and their corresponding masks into a lower-dimensional latent space. We then estimate a conditional velocity field that guides the flow based on the input image. By sampling multiple latent representations, our method synthesizes diverse segmentation outputs whose pixel-wise variance reliably captures the underlying data distribution, enabling both highly accurate and uncertainty-aware predictions. Furthermore, we generate confidence maps that quantify the model’s certainty, providing clinicians with richer information for deeper analysis. We conduct experiments on two datasets, ISIC-2018 and CVC-Clinic, and compare our method with several prior baselines, including both deterministic and generative approach models. Through comprehensive evaluations, both qualitative and quantitative results show that our approach achieves superior segmentation accuracy while remaining highly efficient in the latent space.

Index Terms—flow-matching, variational autoencoder, medical image segmentation, latent representation

I. INTRODUCTION

Medical image segmentation is a crucial step in diagnosis, treatment planning, and image-guided surgery. It enables clinicians and medical experts to clearly identify and precisely localize abnormal regions such as lesions, tumors, and other pathological structures. Manual segmentation, however, is labor-intensive, time-consuming, and increasingly impractical, motivating the need for automated solutions. With the rapid development of artificial intelligence, a wide range of Deep Learning (DL) models has been applied to medical image segmentation, ranging from convolutional neural network (CNN)-based architectures [1], [4], [8], [11] to more recent transformer-based models [10], [12], [14], [15]. These models typically rely on labeled medical datasets and learn a direct mapping from the input image to its corresponding segmentation mask. Despite these advances, they still struggle with the inherent challenges of medical data, where anatomical structures are often ambiguous and boundaries can be difficult to delineate. As a result, deterministic approaches that produces only a single output be-

comes unreliable, fails to capture uncertainty, and ultimately limits overall performance.

Recently, a new direction has emerged that focuses on learning the underlying data distribution rather than predicting a single deterministic mask. By modeling this distribution, generative approaches can capture richer structural information and produce diverse segmentation outputs. This ability yields more stable and uncertainty-aware predictions, which is crucial in medical imaging where ambiguity and inter-observer variability are common. Although originally developed for image synthesis, generative models have shown strong capacity to learn complex patterns, making them well-suited for segmentation tasks involving noisy or inherently ambiguous data. By sampling multiple segmentation candidates, these models not only express uncertainty but also provide outputs that are often more clinically meaningful. Various generative frameworks have been explored for this purpose, including VAE-based models [5]–[7], generative adversarial network (GANs)-based models [2], [3], diffusion-based models [9], [13], [17], [18]. Even the most recent and prominent FM model [16] has also been adapted for this problem [20], [21]. FM has attracted significant attention due to its ability to learn exact data densities instead of relying on a evidence lower bound (ELBO), providing a promising direction for more accurate and robust segmentation.

In this paper, we further advance FM by introducing LatentFM, a novel flow-based model for medical image segmentation in the latent space. Our method integrates two VAEs to encode both images and masks into a shared latent space, combined with a conditional FM framework that enables the model to segment in this latent space. This design allows our model to effectively learn the underlying mask distribution while sampling multiple times to generate diverse segmentation masks for each input image. These samples can then be ensemble-averaged, producing more stable and reliable predictions compared with previous one-shot approaches. Furthermore, we also provide confidence maps that highlight regions where the model is more or less certain, offering clinicians valuable information for deeper analysis of the detected anatomical or pathological areas.

II. RELATED WORK

Deterministic approach: Deep learning models for medical image segmentation have traditionally followed deterministic paradigm, where each input image is mapped to a single segmentation mask. Representative CNN-based architectures include encoder-decoder networks such as UNet [1], which first introduced skip connections to preserve spatial information; UNet++ [4], which enhances feature fusion via dense nested skip pathways; nnUNet [11], which automatically configures the network architecture and training pipeline; and ResUNet [8], which incorporates residual connections to improve gradient flow and feature learning. In addition, transformer-based variants have recently shown strong performance, including TransUNet [10], SwinUNet [15], SegFormer [12], and UNETR [14]. TransUNet combines a vision transformer encoder with a UNet decoder to capture long-range dependencies while preserving local details. SwinUNet leverages hierarchical Swin Transformer blocks for efficient multi-scale feature extraction. SegFormer employs a lightweight transformer backbone with MLP decoders, achieving strong segmentation performance with fewer parameters. UNETR uses a pure transformer encoder connected to a decoder via skip connections, providing effective volumetric segmentation, especially for 3D medical images. Overall, these models consistently demonstrate improved boundary reconstruction, multi-scale feature representation, and high accuracy across diverse medical imaging datasets. However, deterministic approaches limit the model to producing a single segmentation result for each input image. Medical imaging data often exhibit substantial variations in acquisition devices, noise levels, and pathological characteristics. Consequently, a single output may fail to capture the full range of plausible interpretations. In clinical practice, diagnoses are typically formed through consensus among multiple experts rather than relying on a single viewpoint. This motivates the development of generative approaches, which can produce multiple plausible segmentation outcomes and more effectively represent uncertainty in medical data.

Generative approach: Unlike deterministic models, generative approaches can produce multiple outputs for each input image, thereby capturing a wider range of plausible anatomical variations. Early probabilistic methods include VAE-based architectures such as ProbUNet [5], which models segmentation uncertainty through a conditional latent space, and PHiSeg [6], which introduces a hierarchical VAE to better capture multiscale variability. GAN-based models, such as SegGAN, have also been explored to improve boundary realism and handle complex structural details. In addition, diffusion-based models have demonstrated superior performance in recent studies, beginning with SegDiff [13], one of the earliest works applying diffusion models to general image segmentation, followed by MedSegDiff [17], the first DM model specifically designed for medical image segmentation. Subsequently, the enhanced MedSegDiffv2 [18] has

further improved stability and segmentation fidelity through refined diffusion processes and architectural optimizations. However, these previous generative models still face notable limitations in learning and estimating the underlying data distribution. GAN-based approaches often suffer from instability and mode collapse, making training unreliable, while VAE and diffusion models rely on optimizing a variational bound on the likelihood, which provides only an indirect approximation of the true data distribution. Most recently, FM has emerged as a strong competitor to DM by directly approximating the likelihood function and enabling more stable and efficient generative modeling across various domains, including medical image segmentation. Specifically, FlowSDF [20] leverages flow-based generative modeling to enhance segmentation quality, while another line of work focuses on estimating aleatoric uncertainty using FM formulations [21], offering more reliable and interpretable predictions in clinical settings. In this paper, we further advance the FM framework by introducing a latent space formulation tailored for medical image segmentation, enabling more stable learning of the conditional mask distribution and more diverse segmentation outputs.

III. METHOD

In this section, we present LatentFM, a conditional FM framework operating in the latent space for medical image segmentation. We first introduce conditional FM and describe how it is adapted to address the segmentation task. Next, we design two VAEs to encode both images and masks into their respective latent spaces while also providing the means to decode the model's outputs. Finally, we integrate these components to learn the conditional mask distribution and perform segmentation indirectly through the latent domain, as shown in Fig. 1.

A. Segmentation via Flow-matching

FM is a deep generative modeling framework originally developed for high fidelity image synthesis. Unlike traditional generative models that rely on optimizing a ELBO loss function, FM directly maximizes the data likelihood by learning a continuous velocity field that transports a simple prior distribution toward the data distribution. This formulation enables FM to better capture fine-grained structures and to approximate the true data density more accurately. For the medical image segmentation task, we consider a supervised dataset

$$\mathcal{D} = \{(X^{(i)}, S^{(i)})\}_{i=1}^N, \quad (1)$$

where $X^{(i)} \in \mathbb{R}^{H \times W \times C}$ denotes the i -th medical image, $S^{(i)} \in \{0, 1\}^{H \times W}$ is its corresponding segmentation mask, and N is the total number of image-mask pairs.

To model the conditional segmentation distribution $q(S | X)$, we adapt the FM framework [16], [19] to generate segmentation masks conditioned on the input image X . Specifically, we construct a time-dependent probability path $\{p_t(S | X)\}_{t \in [0, 1]}$ that transports a simple source distribution $p_0(S)$ (e.g., an isotropic Gaussian) toward the target

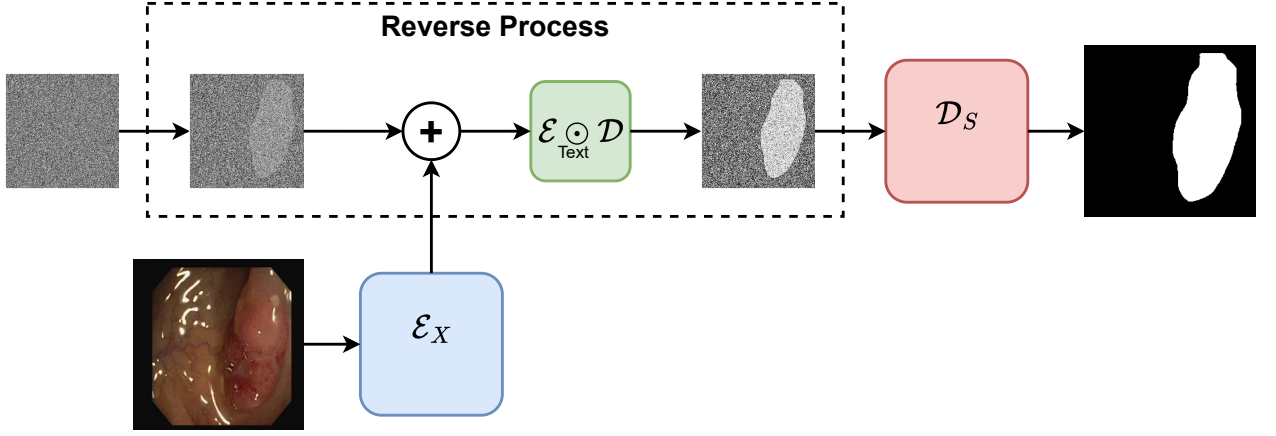


Figure 1. Illustration of our pipeline for conditional FM-based segmentation during the reverse process.

distribution $p_1(S) = q(S | X)$. We also define a flow ψ_t that evolves a source sample $S_0 \sim p_0$ according to the ordinary differential equation

$$\frac{d}{dt} \psi_t(S_0) = u_\theta(t, \psi_t(S_0), X), \quad S_t = \psi_t(S_0), \quad (2)$$

where $u_\theta(t, S_t, X)$ is a learnable, time-dependent velocity field conditioned on the image X . The start state $S_0 = \psi_0(S_0)$ and the terminal state $S_1 = \psi_1(S_0)$ are respectively distributed according to the source distribution $p_0(S)$ and the target conditional distribution $q(S | X)$. To learn this velocity field, we introduce a conditioning latent variable z along the probability path $\{p_t(S | X, z)\}_{t \in [0,1]}$. The marginal segmentation distribution is obtained by integrating over z :

$$p_t(S | X) = \int p_t(S | X, z) p(z | X) dz, \quad (3)$$

Following the FM framework [16], [19], one convenient choice is to condition the velocity field on both the source and target points. In this setting, we define the latent variable z as

$$z = (S_0, S_1) \sim p(z | X) = p_0(S) q(S | X), \quad (4)$$

where $S_0 \sim \mathcal{N}(0, I)$ is the source sample and S is the ground-truth segmentation mask associated with the input image X . Among the possible probability paths, we adopt the concentrated Gaussian path that linearly interpolates between S_0 and S . For a fixed standard deviation σ , the conditional probability path is defined as

$$p_t(S | X, z = (S_0, S_1)) = \mathcal{N}((1-t)S_0 + tS_1, \sigma^2 I), \quad (5)$$

with boundary conditions

$$p_{t=0}(S | X, z) = p_0(S), \quad (6)$$

$$p_{t=1}(S | X, z) = \delta(S - S_1). \quad (7)$$

with δ denoting the Dirac delta distribution. As $\sigma \rightarrow 0$, the Gaussian collapses to this Dirac path and satisfies the exact

boundary constraints. In our formulation, the segmentation mask at time t is given by the straight line interpolation

$$S_t = (1-t)S_0 + tS_1, \quad (8)$$

and learning the velocity field reduces to a regression problem with the ground-truth velocity

$$u(t, S_t, X) = S_1 - S_0. \quad (9)$$

Accordingly, our loss function is defined

$$\mathcal{L} = \mathbb{E}_{t, X, S_0, S_1} [\|u_\theta(t, S_t, X) - (S_1 - S_0)\|^2], \quad (10)$$

where $t \sim \mathcal{U}(0, 1)$, X is the input image that is drawn from the dataset, and S_0, S_1 is drawn following Equation 4.

Once the conditional FM model is trained, a segmentation map S_1 is obtained by integrating the velocity field:

$$S_1 = \psi_1(S_0, X), \quad S_0 \sim p_0(S). \quad (11)$$

Furthermore, multiple segmentation samples can be generated by drawing different source samples $\{S_0^{(i)}\}_{i=1}^n$ and propagating each through the learned flow:

$$S_1^{(i)} = \psi_1(S_0^{(i)}, X), \quad i = 1, \dots, n. \quad (12)$$

The variability among the set $\{S_1^{(i)}\}_{i=1}^n$ can be quantified using the pixel-wise variance, which provides a confidence map reflecting the model's uncertainty. In addition, by thresholding the averaged predictions at 0.5, we obtain the ensemble segmentation mask, yielding a more stable and reliable final prediction.

B. Image and Mask in the latent space

We utilize the VAE [7] framework to construct two encoder-decoder models for medical images and their corresponding masks. First, we obtain a compact latent representation of the medical images through the image VAE. The image encoder \mathcal{E}_X maps an input image $X \in \mathbb{R}^{H \times W \times C}$ to a latent code $z_X = \mathcal{E}_X(X)$, while the decoder \mathcal{D}_X reconstructs the image $X' = \mathcal{D}_X(z_X)$. The latent tensor $z_X \in \mathbb{R}^{h \times w \times c}$

lies in a lower-dimensional space, where the encoder down-samples the resolution by a factor $f = H/h = W/w$. We evaluate several downsampling scales $f = 2^m$ with $m \in \mathbb{N}$.

For details, we assume $X \sim p(X)$. A latent-variable generative model defines a joint distribution over (X, z_X) , with prior $p(z_X)$ and likelihood $p_\theta(X | z_X)$. The maximum marginal likelihood objective is

$$\mathbb{E}_{p(X)}[\log p_\theta(X)] = \mathbb{E}_{p(X)}[\log \mathbb{E}_{p(z_X)}[p_\theta(X | z_X)]] . \quad (13)$$

Since the true posterior $p_\theta(z_X | X)$ is intractable, we introduce a variational approximation $q_\phi(z_X | X)$, leading to the ELBO loss function:

$$\mathcal{L}_{\text{ELBO}}(X) = \mathbb{E}_{q_\phi(z_X | X)}[\log p_\theta(X | z_X)] - D_{\text{KL}}(q_\phi(z_X | X) \| p(z_X)) . \quad (14)$$

Averaging this objective over the dataset yields:

$$\mathcal{L}_{\text{ELBO}} = \mathbb{E}_{p(X)}[\mathcal{L}_{\text{rec}}] - \mathbb{E}_{p(X)}[\mathcal{L}_{\text{reg}}] . \quad (15)$$

While this VAE models the image distribution $p(X)$, we also require a compact latent representation for segmentation masks. Therefore, we introduce a second VAE with encoder \mathcal{E}_S and decoder \mathcal{D}_S , mapping a mask S to a latent code $z_S = \mathcal{E}_S(S)$ and reconstructing it via $\mathcal{D}_S(z_S)$. The mask VAE is trained with the analogous ELBO, which provides a smooth, structured latent space for masks. These latent variables will be used in the latent FM model described next.

C. Segmentation via Latent Flow-matching

With the two VAE models, both the medical image and the segmentation mask are mapped into their respective latent spaces, yielding latent codes $z_X = \mathcal{E}_X(X)$ and $z_S = \mathcal{E}_S(S)$. In this latent domain, we incorporate the conditional FM framework to model the latent conditional mask distribution $q(z_S | z_X)$. Formally, we learn a velocity field $u_\theta(t, z_t, z_X)$, following the setup in Section III-A, which drives a latent flow $z_t = \psi_t(z_0)$ from a source latent sample $z_0 \sim p_0(z)$ toward the target latent mask $z_1 = z_S$. Similar to the pixel-space formulation, when σ approaches zero the concentrated Gaussian path collapses to a Dirac distribution and satisfies the exact boundary conditions. In our latent formulation, the trajectory at time t is therefore given by the straight-line interpolation

$$z_t = (1 - t) z_0 + t z_S . \quad (16)$$

This flow transports samples drawn from the simple prior distribution $p_0(z)$ to the conditional latent mask distribution $q(z_S | z_X)$, enabling the model to generate mask embeddings that are aligned with the latent image representation z_X . Learning this velocity field reduces to a regression problem with the ground-truth velocity

$$u(t, z_t, z_X) = z_S - z_0 . \quad (17)$$

Accordingly, our loss function is defined as

$$\mathcal{L} = \mathbb{E}_{t, z_X, z_0, z_S} [\|u_\theta(t, z_t, z_X) - (z_S - z_0)\|^2] , \quad (18)$$

where $t \sim \mathcal{U}(0, 1)$, $z_X = \mathcal{E}_X(X)$ is the image latent code, $z_0 \sim p_0(z)$ is a source latent sample drawn from the prior distribution, and $z_S = \mathcal{E}_S(S)$ represents the latent mask corresponding to the ground-truth segmentation of image X . Similarly, by reversing the process in Eqs. 11 and 12, we can sample output segmentation masks for each image. In addition, we incorporate the mask decoder \mathcal{D}_S at the end to decode the latent representation back to the original mask space. The entire segmentation pipeline is illustrated in Fig. 1, where we can iteratively sample multiple segmentation outputs for a given medical image. These samples are then used to produce a confidence map and a more stable, more reliable averaged output mask.

IV. EXPERIMENTS

A. Dataset

We conducted experiments on two medical image datasets. The first dataset was ISIC-2018, a large-scale collection of dermoscopic images from the International Skin Imaging Collaboration challenge, focusing on melanoma detection and segmentation. We used 3,694 paired dermoscopic images and masks, split into 3,194 for training, 250 for validation, and 250 for testing. The second dataset was CVC-ClinicDB, a widely used benchmark for polyp segmentation in colonoscopy images, containing 612 image-mask pairs. We divided this dataset into 492 training samples, 60 validation samples, and 60 testing samples. For both datasets, we resized all images to a spatial resolution of 256×256 pixels and normalized them to the range $[-1, 1]$ using a standard preprocessing scheme with mean 0.5 and standard deviation 0.5, ensuring consistent input dimensions and stable optimization during training.

B. Implementation Details

We implemented two main types of models: two VAE models and a conditional FM model. First, we employed a VAE to encode image data from the original image space into a lower-dimensional latent representation. In both the ISIC-2018 and CVC-ClinicDB datasets, input images had an initial resolution of 256×256 . Medical images were represented as $[256 \times 256 \times 3]$ and segmentation masks as $[256 \times 256 \times 1]$. The VAE used a base channel size of 64 with channel multipliers $[1, 2, 4]$, and each stage consisted of residual and attention blocks. After encoding, both the image and its corresponding mask were projected into a latent space of size $[64 \times 64 \times 3]$. We trained the VAE for 250 epochs with a learning rate of 1×10^{-5} and a batch size of 4. Building on these latent embeddings, we implemented a conditional latent flow-matching model using a UNet architecture with a base channel size of 64 and channel multipliers $[1, 2, 2, 4]$. Each stage again incorporated residual and attention blocks. We trained the model for 250 epochs with a fixed learning rate of 1×10^{-5} . During inference, we performed five sampling iterations to simulate the decision variability of five clinicians, following the same protocol as MedSegDiff [17].

We applied all hyperparameters consistently across both datasets.

C. Results

We evaluated the two main components of our framework: the VAE models for both images and masks, and the conditional FM model for latent-space segmentation. The VAE results demonstrated stable and reliable reconstruction performance, as shown in Tab. I. For image reconstruction, the VAE achieved an SSIM of 0.88 and a PSNR of 32.84 on ISIC-2018, and an SSIM of 0.90 with a PSNR of 33.56 on CVC-ClinicDB. These results indicated that the latent representations extracted from images were sufficiently informative to guide the downstream segmentation process. For mask reconstruction, the VAE consistently produced highly accurate results, reaching 0.99 Dice and IoU on both datasets, along with SSIM scores above 0.98 and PSNR values above 34. These strong reconstruction metrics confirmed that the mask distributions were easier to model and that the learned latent space effectively captured the essential structural information. Overall, the VAE provided a stable latent embedding that facilitated effective encoding and decoding for the segmentation outputs generated by the latent FM model.

Table I
RECONSTRUCTION RESULTS OF VAEs FOR BOTH IMAGES AND SEGMENTATION MASKS

| Dataset | Input | Dice | IoU | SSIM | PSNR |
|--------------|-------|------|------|------|-------|
| ISIC-2018 | Mask | 0.99 | 0.99 | 0.98 | 34.24 |
| | Image | – | – | 0.88 | 32.84 |
| CVC-ClinicDB | Mask | 0.99 | 0.99 | 0.99 | 36.04 |
| | Image | – | – | 0.90 | 33.56 |

For the segmentation task, we compared our method with prior models from two major categories: deterministic and generative approaches, as shown in Tab. II. Generative methods consistently outperformed deterministic baselines, yielding more accurate and reliable segmentation results. Among deterministic models, UNet and UNet++ produced moderate results and ranked lowest. More advanced architectures such as nnUNet and TransUNet achieved noticeably better performance. TransUNet exhibited stable results across both datasets, achieving Dice scores of 0.89 and 0.90 and IoU scores of 0.83 and 0.85 on ISIC-2018 and CVC-ClinicDB, respectively. nnUNet performed strongly on ISIC-2018 but showed weaker generalization on CVC-ClinicDB.

In additional, we compare with generative approach models and provide both qualitative and quantitative results, as shown in Fig. 2 and Tab. II. The qualitative results indicate that DM struggles around mask boundaries and faces challenges in ambiguous cases, such as lesion regions with hair in the ISIC-2018 dataset. The subsequent models, FM and LatentDiff, produce more stable reconstructions with higher consistency across masks. The best performance is achieved by LatentFM, whose confidence map exhibits

Table II
COMPARISON OF THE PROPOSED MODEL WITH PREVIOUS DETERMINISTIC AND GENERATIVE APPROACHES.

| Model | ISIC-2018 | | CVC-ClinicDB | |
|---|---------------|---------------|---------------|---------------|
| | Dice | IoU | Dice | IoU |
| Deterministic Segmentation Methods | | | | |
| UNet | 0.8359 | 0.7550 | 0.8313 | 0.7469 |
| UNet++ | 0.8100 | 0.7290 | 0.8016 | 0.7236 |
| nnUNet | 0.9080 | 0.8360 | 0.8130 | 0.7330 |
| TransUNet | 0.8940 | 0.8220 | 0.9180 | 0.8590 |
| Generative Segmentation Methods | | | | |
| DM | 0.8709 | 0.7714 | 0.8244 | 0.7313 |
| LatentDM | 0.9130 | 0.8410 | 0.8956 | 0.8111 |
| FM | 0.9101 | 0.8399 | 0.8902 | 0.8100 |
| LatentFM | 0.9511 | 0.9067 | 0.9371 | 0.8816 |

smooth variations that clearly reflect the model’s consensus and certainty. Aligned with the quantitative results, DM outperformed weaker deterministic baselines but remained slightly below TransUNet on average. LatentDM surpassed all deterministic models on ISIC-2018 with Dice 0.91 and IoU 0.84 but performed less strongly on CVC-ClinicDB. In contrast, FM-based model delivered notably stronger results than diffusion models due to their more accurate approximation of the target distribution. Our proposed LatentFM achieved the best overall performance, reaching Dice scores of 0.9511 and 0.9371 and IoU scores of 0.9067 and 0.8816 on ISIC-2018 and CVC-ClinicDB, respectively. Compared to LatentDM, LatentFM improved Dice by more than 0.04 and IoU by over 0.06 on both datasets. These results highlight that the generative approach is better suited for medical image segmentation, and our proposed LatentFM, which models data distributions indirectly through the latent space, achieves the best performance and greater efficiency among methods following this direction.

V. CONCLUSION

In this paper, we addressed the medical image segmentation problem from a generative modeling perspective. Inspired by the strengths of FM, we extended and adapted this framework for segmentation tasks. Specifically, we designed a pair of VAEs to encode both medical images and masks into a compact latent space. Using these latent representations, our conditional FM module learned the latent mask distribution conditioned on the image latent code, effectively guiding the segmentation process. Consequently, the model generated multiple plausible segmentation masks for each input image, from which we derived confidence maps and ensemble-averaged predictions, resulting in more stable and reliable outputs. Experimental results showed that LatentFM consistently outperformed existing baselines, including both deterministic models and prior generative approaches. LatentFM achieved superior performance on both datasets while providing meaningful uncertainty estimation. In the future, we plan to further explore this direction by developing

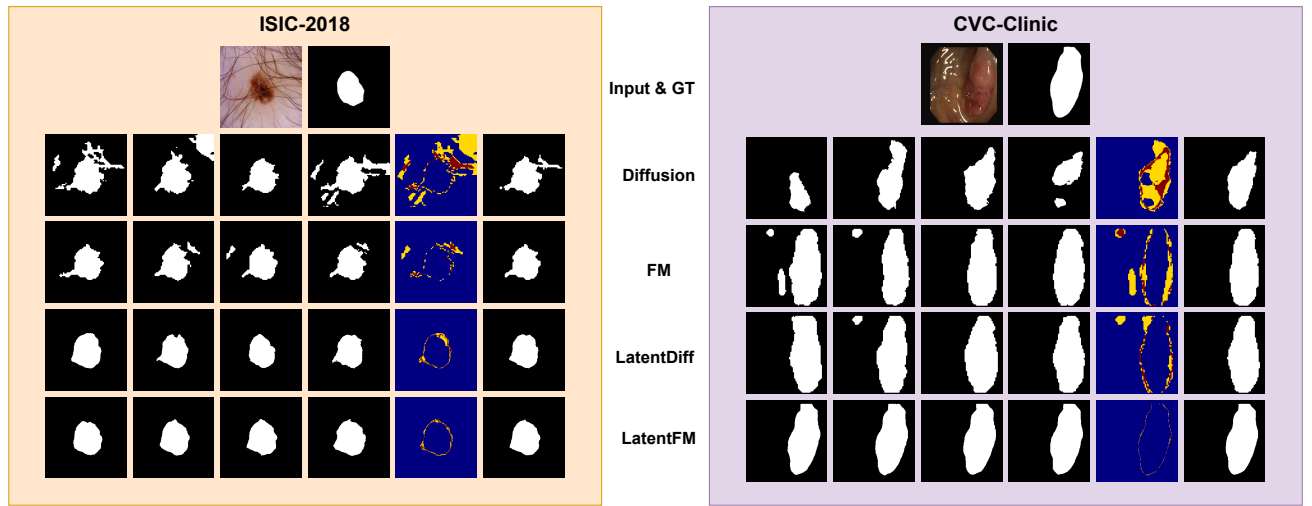


Figure 2. Qualitative comparison between our proposed LatentFM and other generative baseline approaches. For each model, the first four columns show the initial segmentation outputs, followed by the corresponding confidence map and the averaged output mask.

more comprehensive uncertainty quantification mechanisms, including explicit modeling of both epistemic and aleatoric uncertainty, to better address the inherent ambiguity in medical imaging tasks.

REFERENCES

- [1] Ronneberger, O., Fischer, P., Brox, T., 2015. U-Net: Convolutional networks for biomedical image segmentation. In: Medical Image Computing and Computer-Assisted Intervention – MICCAI 2015. Springer, pp. 234–241.
- [2] Goodfellow, I., Pouget-Abadie, J., Mirza, M., Xu, B., Warde-Farley, D., Ozair, S., Courville, A., Bengio, Y., 2014. Generative adversarial nets. In: Advances in Neural Information Processing Systems 27 (NeurIPS).
- [3] Xue, Y., Xu, T., Zhang, H., Long, L.R., Huang, X., 2018. SegAN: Adversarial network with multi-scale L1 loss for medical image segmentation. *Neuroinformatics* 16 (3), 383–392.
- [4] Zhou, Z., Rahman Siddiquee, M.M., Tajbakhsh, N., Liang, J., 2018. UNet++: A nested U-Net architecture for medical image segmentation. In: Deep Learning in Medical Image Analysis and Multimodal Learning for Clinical Decision Support. Springer, pp. 3–11.
- [5] Kohl, S., Romera-Paredes, B., Meyer, C., De Fauw, J., Ledsam, J.R., Maier-Hein, K., Eslami, S.M.A., Jimenez Rezende, D., Ronneberger, O., 2018. A probabilistic U-Net for segmentation of ambiguous images. In: Advances in Neural Information Processing Systems 31 (NeurIPS).
- [6] Baumgartner, C.F., Tezcan, K.C., Chaitanya, K., Hötker, A.M., Muehlematter, U.J., Schawkat, K., Becker, A.S., Donati, O., Konukoglu, E., 2019. PHISeg: Capturing uncertainty in medical image segmentation. In: Medical Image Computing and Computer-Assisted Intervention – MICCAI 2019. Springer, pp. 119–127.
- [7] Kingma, D.P., Welling, M., 2019. An introduction to variational autoencoders. *Foundations and Trends in Machine Learning* 12 (4), 307–392.
- [8] Diakogiannis, F.I., Waldner, F., Caccetta, P., Wu, C., 2020. ResUNet-a: A deep learning framework for semantic segmentation of remotely sensed data. *ISPRS Journal of Photogrammetry and Remote Sensing* 162, 94–114.
- [9] Ho, J., Jain, A., Abbeel, P., 2020. Denoising diffusion probabilistic models. In: Advances in Neural Information Processing Systems 33 (NeurIPS), pp. 6840–6851.
- [10] Chen, J., Lu, Y., Yu, Q., Luo, X., Adeli, E., Wang, Y., Lu, L., Yuille, A.L., Zhou, Y., 2021. TransUNet: Transformers make strong encoders for medical image segmentation. *arXiv preprint arXiv:2102.04306*.
- [11] Isensee, F., Jaeger, P.F., Kohl, S.A.A., Petersen, J., Maier-Hein, K.H., 2021. nnU-Net: a self-configuring method for deep learning-based biomedical image segmentation. *Nature Methods* 18 (2), 203–211.
- [12] Xie, E., Wang, W., Yu, Z., Anandkumar, A., Alvarez, J.M., Luo, P., 2021. SegFormer: Simple and efficient design for semantic segmentation with transformers. In: Advances in Neural Information Processing Systems 34 (NeurIPS), pp. 12077–12090.
- [13] Amit, T., Shaharbany, T., Nachmani, E., Wolf, L., 2021. SegDiff: Image segmentation with diffusion probabilistic models. *arXiv preprint arXiv:2112.00390*.
- [14] Hatamizadeh, A., Tang, Y., Nath, V., Yang, D., Myronenko, A., Landman, B., Roth, H.R., Xu, D., 2022. UNETR: Transformers for 3D medical image segmentation. In: Proceedings of the IEEE/CVF Winter Conference on Applications of Computer Vision, pp. 574–584.
- [15] Cao, H., Wang, Y., Chen, J., Jiang, D., Zhang, X., Tian, Q., Wang, M., 2022. Swin-Unet: Unet-like pure transformer for medical image segmentation. In: European Conference on Computer Vision (ECCV), Springer, pp. 205–218.
- [16] Lipman, Y., Chen, R.T.Q., Ben-Hamu, H., Nickel, M., Le, M., 2022. Flow matching for generative modeling. *arXiv preprint arXiv:2210.02747*.
- [17] Wu, J., Fu, R., Fang, H., Zhang, Y., Yang, Y., Xiong, H., Liu, H., Xu, Y., 2024. MedSegDiff: Medical image segmentation with diffusion probabilistic model. In: Medical Imaging with Deep Learning (MIDL), PMLR, pp. 1623–1639.
- [18] Wu, J., Ji, W., Fu, H., Xu, M., Jin, Y., Xu, Y., 2024. MedSegDiff-V2: Diffusion-based medical image segmentation with transformer. In: Proceedings of the AAAI Conference on Artificial Intelligence 38 (6), pp. 6030–6038.
- [19] Lipman, Y., Havasi, M., Holderrieth, P., Shaul, N., Le, M., Karrer, B., Chen, R.T.Q., Lopez-Paz, D., Ben-Hamu, H., Gat, I., 2024. Flow matching guide and code. *arXiv preprint arXiv:2412.06264*.
- [20] Bogensperger, L., Narnhofer, D., Falk, A., Schindler, K., Pock, T., 2025. FlowSDF: Flow matching for medical image segmentation using distance transforms. *International Journal of Computer Vision*, 1–13.
- [21] Nguyen, V.P., Trinh, N.H., Nguyen, D.M.L., Nguyen, P.L., Tran, Q.L., 2025. Aleatoric uncertainty medical image segmentation estimation via flow matching. In: International Workshop on Uncertainty for Safe Utilization of Machine Learning in Medical Imaging. Springer, pp. 134–144.